BIOCHEMISTRY
including biophysical chemistry & molecular biology

Article

pubs.acs.org/biochemistry

Demonstration of Ligand Decoration, and Ligand-Induced Perturbation, of G-Quadruplexes in a Plasmid Using Atomic Force Microscopy

Ioanna Mela,[†] Ramon Kranaster,[‡,§] Robert M. Henderson,[†] Shankar Balasubramanian,[‡,§,∥] and J. Michael Edwardson*[,†]

[†]Department of Pharmacology, University of Cambridge, Tennis Court Road, Cambridge CB2 1PD, U.K.

[‡]Department of Chemistry, University of Cambridge, Lensfield Road, Cambridge CB2 1EW, U.K.

[§]Cancer Research UK, Cambridge Research Institute, Li Ka Shing Center, Cambridge CB2 0RE, U.K.

[∥]School of Clinical Medicine, University of Cambridge, Cambridge CB2 0SP, U.K.

Supporting Information

ABSTRACT: G-Quadruplexes are nucleic acid secondary structures consisting of a planar arrangement of four guanine residues. Potential G-quadruplex-forming sequences are widely distributed throughout the genome. Significantly, they are present in telomeres and are enriched in gene promoters and first introns, raising the possibility that perturbation of G-quadruplex stability might have therapeutic potential, for example in the treatment of cancer. Ligands that interact selectively with G-quadruplexes include both proteins and small molecules, although the interactions between ligands and their G-quadruplex targets have been monitored using indirect methods. In addition, the G-quadruplex targets have often been short DNA fragments. Here, we have used atomic force microscopy imaging to examine directly at the single-molecule level the interaction of ligands with G-quadruplexes generated during transcription of a plasmid containing a G-rich insert. We show that the structures produced during transcription are decorated specifically by the single-chain antibody HF1 and by the nuclear protein PARP-1, both of which are known to recognize G-quadruplexes. Our results provide clear structural evidence of G-quadruplex formation in a transcription-dependent case and demonstrate directly how small-molecule stabilizers and destabilizers can manipulate these structures in a biochemically functional system.

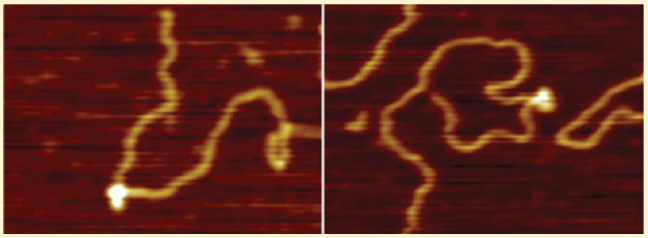

G-Quadruplexes are nucleic acid secondary structures consisting of a planar arrangement of four guanine residues that interact via Hoogsteen hydrogen bonds and are stabilized by monovalent cations (reviewed in refs 1 and 2). Sequences that are predicted to form G-quadruplexes are widely distributed throughout the genome.[3] Significantly, they are present in the telomeres at the ends of chromosomes[4,5] and are also enriched in gene promoters,[6−8] suggesting that they may play roles in the control of replication competence and gene transcription, respectively.[9−11] In turn, these putative functions of G-quadruplexes raise the possibility that perturbation of G-quadruplex stability might have therapeutic potential, for example in the treatment of cancer (reviewed in refs 2 and 12).

Many ligands that interact selectively with G-quadruplexes have now been described (reviewed in refs 2 and 12); these include proteins, such as nucleolin and ribonucleolin,[13] the helicase Pif1,[14] and artificial antibodies,[15] as well as small molecules (reviewed in ref 16). Of particular interest to us in the context of this study is the fact that the single-chain variable fragment antibody HF1 binds to various G-quadruplexes with dissociation constants in the nanomolar to micromolar range but shows much weaker binding to double-stranded DNA.[17] HF1 has exhibited G-quadruplex-associated function in budding yeast[5] and in human cells.[17] In addition, the abundant nucleoprotein poly(ADP-ribose) polymerase-1 (PARP-1) is known to bind to G-quadruplexes with high affinity and to become activated upon binding.[18] Many small-molecule ligands that show preferential binding to G-quadruplexes have been synthesized. These include the pyridine-2,6-bis-quinolinodicarboxamide derivative pyridostatin[19,20] and the triarylpyridine molecule TAP1.[21] The structures of these two compounds are shown in Figure 1. Significantly, the two ligands have opposite effects on G-quadruplex stability, with pyridostatin having a stabilizing effect[19,22] and TAP1 causing destabilization.[21]

Until now, the interactions between ligands and their G-quadruplex targets have been monitored largely by biophysical methods, such as enzyme-linked immunosorbent assays,[23] surface plasmon resonance,[19] circular dichroism (CD) spec-

Received: October 19, 2011
Revised: December 21, 2011
Published: December 22, 2011

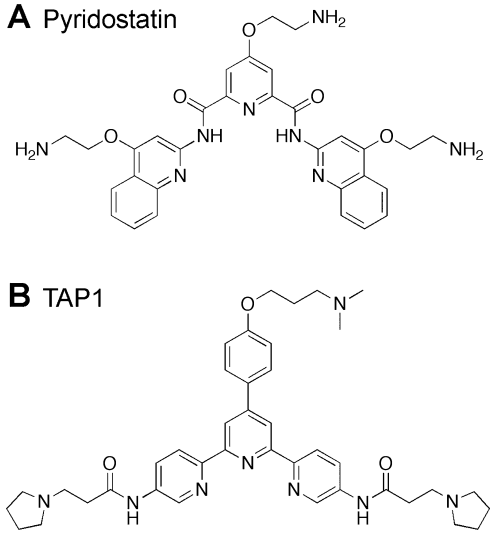

Figure 1. Structures of pyridostatin (A) and TAP1 (B).

troscopy,[21,23] and nuclear magnetic resonance (NMR) spectroscopy,[20,21] using short synthetic DNA oligonucleotides.[19−21,23−27] What is lacking is a detailed examination of the interaction of these ligands with G-quadruplexes at the single-molecule level in the context of a more biologically relevant DNA molecule.

Atomic force microscopy (AFM) can be used to image DNA at the single-molecule level with only minimal sample preparation.[28−30] We have recently used AFM to examine the structures produced when a plasmid containing a G-rich coding strand was transcribed in vitro.[31] Specifically, we imaged stable RNA−DNA hybrid loops generated by transcription of plasmid pPH600, which contains a 597 bp fragment of the murine immunoglobulin Sγ3 switch region.[32] We found that the non-RNA-containing portion folded into structures that we interpreted as G-quadruplexes.[31] After in vitro transcription, almost all of the plasmids had an asymmetric loop, a large asymmetric blob, or a spurlike projection at the appropriate position on the DNA contour. These structures disappeared after treatment of the transcribed plasmid with RNase H, which removes mRNA hybridized with the template strand. Replacement of K^+ in the transcription buffer with either Na^+ or Li^+ caused a reduction in the percentage of plasmids containing the structures, consistent with the known effects of these cations on G-quadruplex stability.[33] In addition to imaging the G-quadruplexes, we examined the effect of G-loop formation on subsequent transcription. Our results indicate that G-loops do not form after only a single round of transcription; rather, they form stochastically but once formed prevent further transcription, suggesting that they might have a regulatory role in vivo.

In our previous study, we provided indirect evidence that the structures we were imaging contained G-quadruplexes. This evidence included the position of the structure on the DNA contour, the dependence of the stability of the structure on the presence of hybridized mRNA on the opposing strand, and the effect of varying the monovalent cation on the stability of the structure. However, in such studies, the nonduplex structures formed were dependent on putative G-quadruplex-forming sequences, but the evidence of G-quadruplex formation was implicit. In this study, we set out to demonstrate directly that G-quadruplexes are formed within the transcribed region of a plasmid in a manner that is transcriptionally dependent using decoration by HF1 and PARP-1 and to examine the effects of the small-molecule ligands, pyridostatin and TAP1, on G-quadruplex stability. Our results now provide three pieces of explicit structural evidence. (1) G-Quadruplex formation takes place in a transcription-dependent case. (2) Ligands interact directly with the G-quadruplex structure. (3) Small-molecule stabilizers and destabilizers can manipulate these G-quadruplex structures in a biochemically functional system.

MATERIALS AND METHODS

G-Quadruplex Ligands. Pyridostatin was synthesized and purified as described by Rodriguez et al.[19] TAP1 was synthesized and purified as described by Waller et al.[21] HF1 was overexpressed, purified, and checked for binding activity against one repeat of the murine Sγ3 switch region by an enzyme-linked immunosorbent assay, as described by Fernando et al.[23]

DNA Substrate. The plasmid used in these experiments, pPH600 (kindly provided by N. Maizels), is a derivative of pBluescript KS(+) (2958 bp). The pPH600 plasmid (3555 bp) has a 597 bp fragment of the murine Sγ3 switch region, which contains the repeat d-(CTGGGCAGCTCTGGGGGAGCTGGGGTAGGTTGG-GAGTGTGGGGACCAGG), inserted just downstream of the T7 promoter.[32] The insert sequence was checked by CD and thermal difference spectroscopy for its G-quadruplex forming potential. Spectra can be seen in Figure S1 of the Supporting Information.

In Vitro Transcription. pPH600 was incubated for 30 min at 37 °C in a buffer solution containing 200 μg/mL DNA, 40 mM Tris-HCl (pH 7.9), 6 mM $MgCl_2$, 10 mM dithiothreitol, 2 mM spermidine, 40 mM KCl, ATP, UTP, GTP, and CTP (1 mM each), and 1 unit/μL T7 polymerase. The sample was then subjected to a 20 min RNase A treatment to digest free mRNA and was subsequently purified using a Qiagen filter. The plasmid was linearized with AflIII before being repurified. Mock transcribed pPH600 plasmid was used as a control. In the case of the experiments with the HF1 antibody and PARP-1, transcribed and linearized plasmids were incubated with the ligand overnight. In the pyridostatin A experiment, hybridized mRNA was removed by treatment of the samples with RNase H for 30 min at 37 °C after the RNase A treatment and before AflIII digestion. Pyridostatin A was present during both transcription and RNase H treatment. TAP1 was added to the transcription buffer as appropriate.

AFM Imaging. Disks of ruby muscovite mica (Goodfellow) were attached to 13 mm steel pucks using Aron Alpha high-strength rapid bonding adhesive, α-cyanoacrylate (Agar Scientific Limited, Essex, U.K.). Immediately prior to DNA deposition, the top layer of the mica was cleaved using Scotch tape to reveal an atomically flat surface. Purified DNA was diluted to a concentration of ~0.5×10^{-14} mol/μL in imaging buffer [10 mM $MgCl_2$ and 10 mM Tris-HCl (pH 7.9)]. Droplets (45 μL) were deposited onto freshly cleaved mica disks and incubated at room temperature for 10 min. Excess DNA was rinsed off with BPC grade water (Sigma-Aldrich, Poole, U.K.), and the water was wicked from the surface using tissue paper. The disks were then dried under a stream of nitrogen gas.

Imaging was performed using a Multimode Nanoscope IIIa atomic force microscope (Bruker AXS, Santa Barbara, CA). All samples were imaged in air using tapping mode with a root-

dx.doi.org/10.1021/bi201600g | Biochemistry 2012, 51, 578−585

mean-square amplitude of ~1.6 V and a drive frequency of ~150 kHz. Commercially available silicon probes with a specified spring constant of 42 N/m were used (Olympus atomic force OMCL-AC160TS-E). Data were gathered by capturing 2 μm by 2 μm scans.

Data Analysis. DNA lengths were measured using Scanning Probe Image Processor, SPIP (Image Metrology A/S). The software recognizes individual DNA molecules and, by drawing a line along the plasmid, calculates the total fiber length.

SPIP was also used for calculation of the volumes of the structures. The edges of each structure were defined by the "circular area of interest" tool, and the volume inside this area was measured. SPIP uses the following equation for the calculation of volume:

$$Z_{\text{net volume}} = Z_{\text{material volume}} - Z_{\text{void volume}}$$

where $Z_{\text{material volume}}$ is the volume of all pixels inside the shape's contour with a Z value greater than or equal to zero:

$$Z_{\text{material volume}} = \sum_{\{Z(x,y)\in \text{shape} | Z\geq 0\}} Z(x, y)\, dx\, dy \quad (1)$$

where dx and dy are the point spacings in the X and Y directions of the image, respectively. $Z_{\text{void volume}}$ is the volume of all pixels inside the shape's contour with a Z value lower than or equal to zero:

$$Z_{\text{void volume}} = \sum_{\{Z(x,y)\in \text{shape} | Z\leq 0\}} Z(x, y)\, dx\, dy \quad (2)$$

where dx and dy are the point spacing in the X and Y directions of the image, respectively.

Volume histograms were drawn with bin widths chosen according to Scott's equation:

$$\text{bin width} = 3.5\sigma/n^{1/3} \quad (3)$$

where σ is an estimate of the standard deviation and n is the sample size.[34] Where Gaussian curves were fitted to the data, the number of curves was chosen to maximize the r^2 value, while giving significantly different means using Welch's t test for unequal sample sizes and unequal variances.[35] All errors quoted are standard errors of the mean (SE).

Molecular volumes of proteins based on molecular mass were calculated using the equation

$$V_c = (M_0/N_0)(V_1 + dV_2) \quad (4)$$

where M_0 is the molecular mass, N_0 is Avogadro's number, V_1 and V_2 are the partial specific volumes of protein and water, respectively, and d is the extent of protein hydration. This equation has been used previously by several groups (e.g., refs 30 and 36–38). The partial specific volume of a typical protein (V_1) is considered to be 0.74 cm^3/g,[39,40] and the extent of protein hydration (d) has been estimated to be 0.4 g of water/g of protein.[41] The partial specific volume of water (V_2), of course, is 1 cm^3/g.

In our early work, we used AFM probes made of silicon nitride. To overcome the large probe-convolution effect, we measured the particle radius at half-height. This method gave a reasonable agreement between measured and predicted molecular volumes. More recently (and in this study), we have used probes made of silicon, which have a higher aspect ratio and a much greater spring constant than the silicon nitride probes. The new probes give a more accurate estimation of the protein volume using the basal radius rather than the half-height radius. Even the new probes generate some lateral broadening; however, this effect is likely mitigated by the reduction in the measured vertical dimension resulting from increased "squashing" of the particles, because of the higher spring constant of the probes. We have recently demonstrated the close correspondence between measured and expected molecular volumes by imaging a range of proteins of known molecular mass.[30]

PARP-1 Activation Assay. Untranscribed or transcribed pPH600 (6 μg/mL) was incubated for 25 min at room temperature in a buffer containing 50 mM Tris-HCl (pH 7.4), 50 mM KCl, 2 mM $MgCl_2$, 1 mM DTT, 50 μM $Zn(OAc)_2$, 133 μM NAD^+, and 10 units of human PARP-1 (HSA-PARP) (Trevigen). Control incubations contained PARP-1 only or no PARP-1. The reactions were stopped by adding sodium dodecyl sulfate–polyacrylamide gel electrophoresis (SDS–PAGE) loading buffer, and samples were heated at 95 °C for 2 min. Samples were analyzed using a 4 to 12% gradient bis-tris polyacrylamide gel (NuPAGE) (Invitrogen). Immunostaining was performed using mouse monoclonal anti-poly(ADP-ribose) antibody 10H (1:1000; Abcam). Proteins were detected by Coomassie blue staining. The unpaired t test was performed using GraphPad Prism.

RESULTS

Decoration of G-Quadruplexes by HF1. We set out to visualize G-loop and G-quadruplex formation by AFM imaging of a plasmid (pPH600) that carries a G-rich 597 bp fragment of the murine Sγ3 switch region.[32] Images of untranscribed, linearized plasmids showed homogeneous spreads of featureless DNA molecules (Figure 2A). The mean length of the molecules (±SE) was 1193 ± 6 nm (n = 36), very close to the expected length of 1173 nm for a 3555 bp plasmid, given a nanometer-to-base pair conversion factor of 0.33 (nm/bp[42]). After in vitro transcription of the plasmids, followed by RNase A treatment (to remove free mRNA) and linearization, the vast majority (80 ± 2%, n = 5 experiments, 136 DNA molecules) of the DNA molecules contained structures that were not present on untranscribed DNA (arrowheads in Figure 2B). The structures observed could be categorized into four groups: blobs, loops, spurs, and double blobs. Examples of each of these structures are shown in Figure 2C–F. We suggest that the blobs (and double blobs) are caused by the aggregation of a small number of closely spaced G-quartets. In the asymmetric loops, the short strand likely represents the G-quadruplex DNA and the longer strand the RNA–DNA hybrid. Spurs would be formed when both sides of the loop attach to the mica surface in an orientation where the loophole is not visible. A frequency distribution of the positions of the structures seen on transcribed plasmids had a single peak at 275 ± 1 nm from the nearer end of the linearized plasmid, consistent with the expected position of the G-rich region of the plasmid.[31,32]

As explained above, single-chain antibody HF1 is known to bind selectively to G-quadruplexes. When in vitro transcription of pPH600 was conducted in the presence of HF1 (0.4 μM), the percentage of plasmids with structures (86 ± 3%, n = 3 experiments, 87 DNA molecules) was not significantly affected. However, when HF1 was added to transcribed DNA, the structures had a different appearance. Specifically, many of the structures now had more than one blob, and the individual blobs appeared larger. A selection of zoomed images of HF1-treated samples is shown in Figure 2G. The change in the

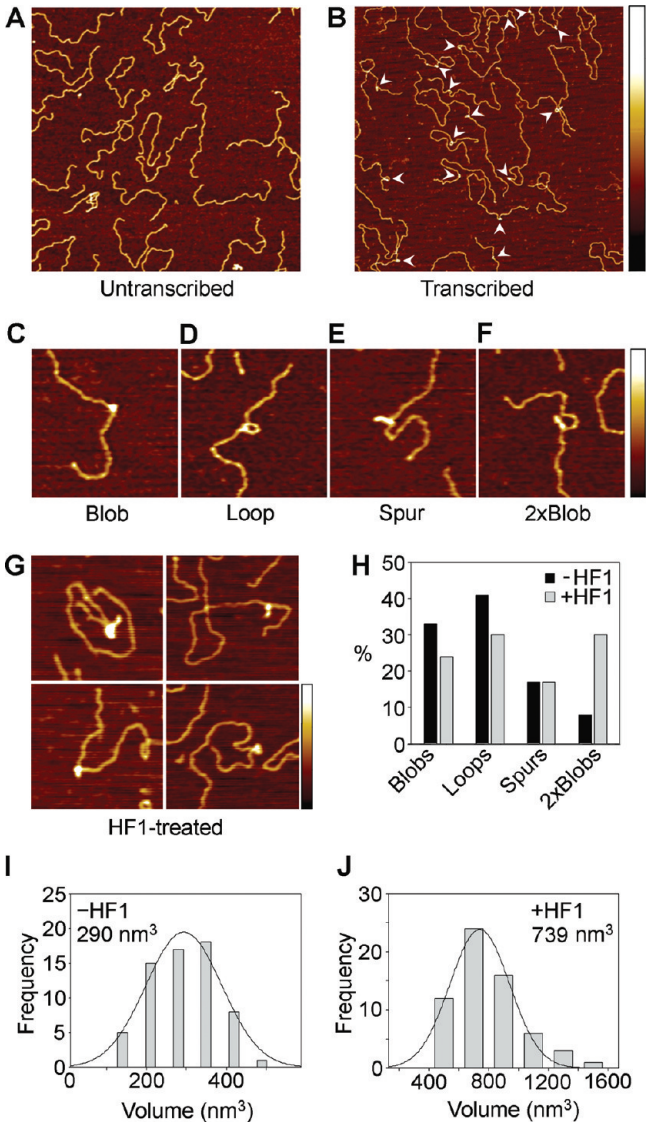

Figure 2. Decoration of G-quadruplexes by HF1. (A and B) Low-magnification (2 μm × 2 μm) AFM images of samples of untranscribed plasmid (A) and transcribed plasmid (B), with positions of structures indicated by arrowheads. The shade height scale is 0−1.4 nm. (C−F) Zoomed (300 nm × 300 nm) images showing a blob (C), a loop (D), a spur (E), and a double blob (F). The shade height scale is 0−1.0 nm. (G) Zoomed (600 nm × 600 nm) images of transcribed plasmids that had been incubated with HF1 (0.4 μM), showing structures decorated with HF1. The shade height scale is 0−1.2 nm. (H) Histogram showing the profiles of structures seen in the absence (black bars; n = 85) and presence (gray bars; n = 71) of HF1. (I and J) Frequency distributions of volumes of structures seen in the absence (I) and presence (J) of HF1. The curves indicate the fitted Gaussian functions. The means of the distributions are indicated.

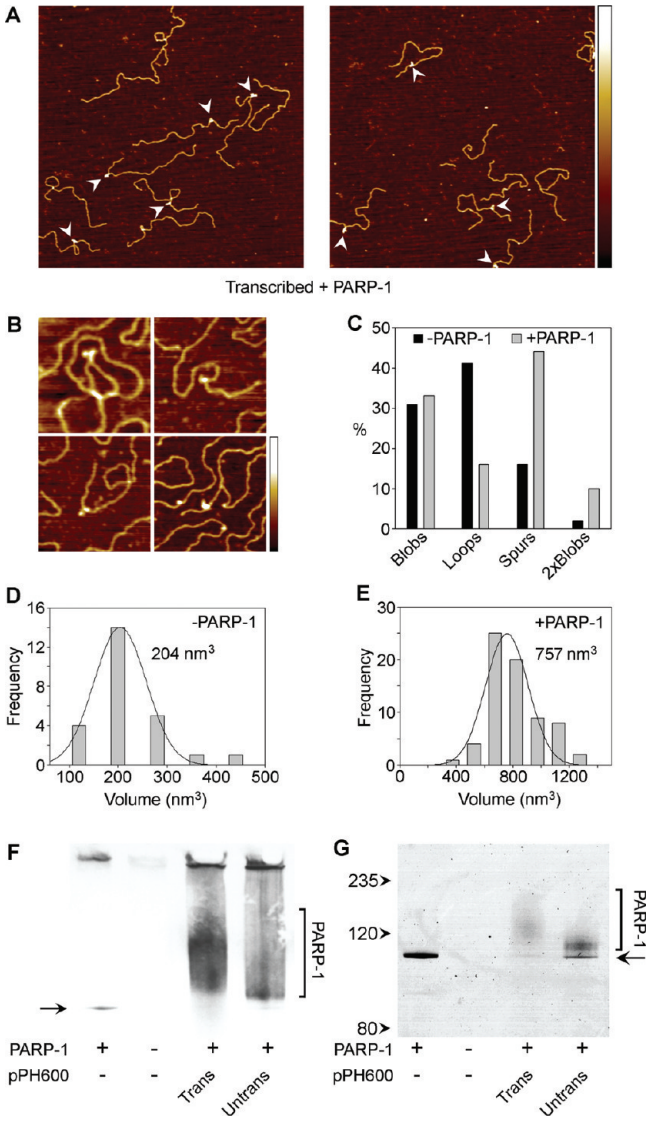

Figure 3. Decoration of G-quadruplexes by PARP-1. (A) Low-magnification (2 μm × 2 μm) AFM images of transcribed plasmids that had been incubated with PARP-1 (90 nM). The positions of structures are indicated by arrowheads. The shade height scale is 0−1.3 nm. (B) Zoomed (600 nm × 600 nm) images showing PARP-1-decorated structures. The shade height scale is 0−1.2 nm. (C) Histogram showing the profile of structures seen in the absence (black bars; n = 88) and presence (gray bars; n = 73) of PARP-1. (D and E) Frequency distributions of volumes of structures seen in the absence (D) and presence (E) of PARP-1. The curves indicate the fitted Gaussian functions. The means of the distributions are indicated. (F) Poly(ADP-ribosyl)ation of PARP-1 in the presence of untranscribed and transcribed pPH600, detected by immunoblotting, using an anti-poly(ADP-ribose) antibody. The arrow indicates automodified PARP-1 bearing a very short chain of PAR, running at ∼113 kDa. (G) Poly(ADP-ribosyl)ation of PARP-1 in the presence of untranscribed and transcribed pPH600, detected by SDS−PAGE, with Coomassie blue staining. Unmodified PARP-1 migrates as a sharp band (arrow); poly(ADP-ribosyl)ated PARP-1 runs as a more slowly migrating smear. Molecular mass markers (kilodaltons) are shown at the left.

appearance of the structures is quantified in Figure 2H. The histogram reveals an increase in the numbers of double blobs after HF1 treatment, and a corresponding decrease in the numbers of single blobs and loops. Panels I and J of Figure 2 show the frequency distributions of volumes of the structures. The peak volume increases from 290 ± 12 nm^3 [n = 79 (Figure 2I)] to 739 ± 18 nm^3 [n = 71 (Figure 2J)] upon HF1 treatment. In a separate experiment, we imaged free HF1 bound to mica and determined the molecular volumes of a number of the particles. A frequency distribution of molecular volumes (Figure S2A of the Supporting Information) had a peak at 58 ± 2 nm^3 (n = 73), close to the predicted size of 50 nm^3 for a protein with a molecular mass of 26 kDa, according to eq 4. Hence, the 449 nm^3 increase in volume indicates that on average approximately seven to eight HF1 molecules are

dx.doi.org/10.1021/bi201600g | *Biochemistry* 2012, 51, 578−585

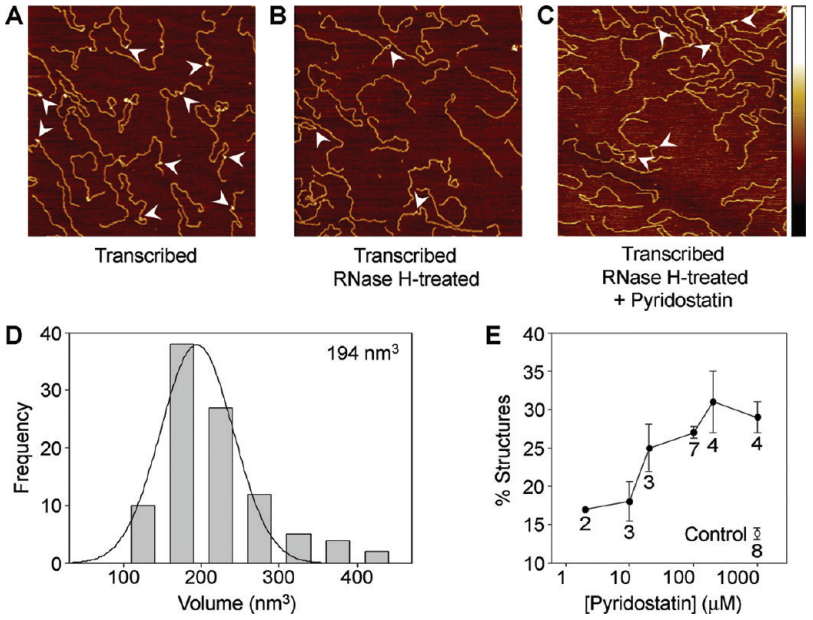

Figure 4. Effect of pyridostatin on G-quadruplex stability. (A) Low-magnification (2 μm × 2 μm) images of transcribed plasmids, with the positions of structures indicated by arrowheads. (B) Low-magnification image of transcribed and RNase H-treated plasmids, with the positions of structures indicated by arrowheads. (C) Low-magnification image of plasmids that had been transcribed and treated with RNase H in the presence of pyridostatin (200 μM). The shade height scale, for panels A–C, is 0–1.3 nm. The positions of structures are indicated by arrowheads. (D) Frequency distribution of volumes of structures seen after RNase H treatment in the presence of pyridostatin A. The curve indicates the fitted Gaussian function. The mean of the distribution is indicated. (E) Dependence of the prevalence of structures on pyridostatin concentration. Control (empty symbol) denotes the percentage of plasmids showing structures in the absence of pyridostatin. Numbers of independent experiments are indicated below the data points.

present within the blobs. This is a reasonable number, given that the online tool *QGRS Mapper*,[43] which was accessed using the interface at http://www.quadruplex.org, predicted that the 597 bp G-rich insert in pPH600 is potentially able to fold into 12 independent G-quadruplexes (Figure S3 of the Supporting Information). We suggest that the observed double blobs, which are rare in the absence of HF1, occur when multiple HF1 molecules bind at distinct locations within this region.

Decoration of G-Quadruplexes by PARP-1. The appearance of the structures observed after transcription of pPH600 was also altered by treatment with the nuclear protein PARP-1 (90 nM), which has been shown previously by others to bind with high affinity to G-quadruplexes.[18] As expected, control (PARP-1-free) images showed the same types of structures as those seen under the HF1-free conditions described above (data not shown). In contrast, in the presence of PARP-1, many spurlike structures were now present (arrowheads in Figure 3A). These are shown in more detail in the zoomed images in Figure 3B. The histogram in Figure 3C shows a decrease in the number of loops and a corresponding increase in the number of spurs. Frequency distributions of volumes of the structures reveal an increase from 204 ± 5 nm^3 [n = 30 (Figure 3D)] to 757 ± 24 nm^3 [n = 73 (Figure 3E)] after addition of PARP-1. Note that the peak volume for the structures in the absence of PARP-1 is lower than the corresponding value in the absence of HF1 (290 nm^3). This difference likely represents the varying efficiency of G-quadruplex formation between experiments. However, the effects of the two proteins (PARP-1 and HF1) on structure volume were assessed within (and not between) experiments. A frequency distribution of molecular volumes of individual PARP-1 molecules bound to mica (Figure S2B of the Supporting Information) had a peak at 192 ± 2 nm^3 (n = 352), close to the predicted size of 215 nm^3 for a protein with a molecular mass of 113 kDa, according to eq 4 (above). Hence, the measured increase in volume (553 nm^3) indicates that on average two to three PARP-1 molecules associate with the structures.

We were interested in discovering whether binding of PARP-1 to the G-quadruplex generated upon transcription of pPH600 resulted in activation of the enzyme. To this end, we incubated PARP-1 with its substrate NAD$^+$ in the presence of either untranscribed or transcribed pPH600. We then subjected the sample to SDS–PAGE followed by immunoblotting, using an antibody against poly(ADP-ribose). Figure 3F shows the result from a typical experiment. As one can see, the presence of the transcribed plasmid produced a more prominent poly(ADP-ribose) signal than the untranscribed plasmid. PARP-1 activation in the absence of DNA was minimal. Using data from three independent experiments, the activation caused by the transcribed plasmid was 1.9 ± 0.3-fold greater than that caused by the untranscribed plasmid (p = 0.004). Because PARP-1 ADP-ribosylates itself, enzyme activation can also be monitored through changes in the migration of PARP-1 on SDS–polyacrylamide gels. As shown in Figure 3G, unmodified PARP-1 runs as a sharp band at ~113 kDa. In contrast, ADP-ribosylated PARP-1 runs more slowly as a smeared band. The gel shows that PARP-1 runs more slowly when it is incubated with transcribed pPH600 than with untranscribed plasmid, again indicating that enzyme activation occurs upon binding of PARP-1 to G-quadruplexes.

Effect of Pyridostatin on G-Quadruplex Stability. Evidence that pyridostatin stabilizes G-quadruplexes has been presented previously.[19,22] To assess the effect of pyridostatin on the G-quadruplexes generated during transcription of pPH600, we treated transcribed plasmids with RNase H in the presence

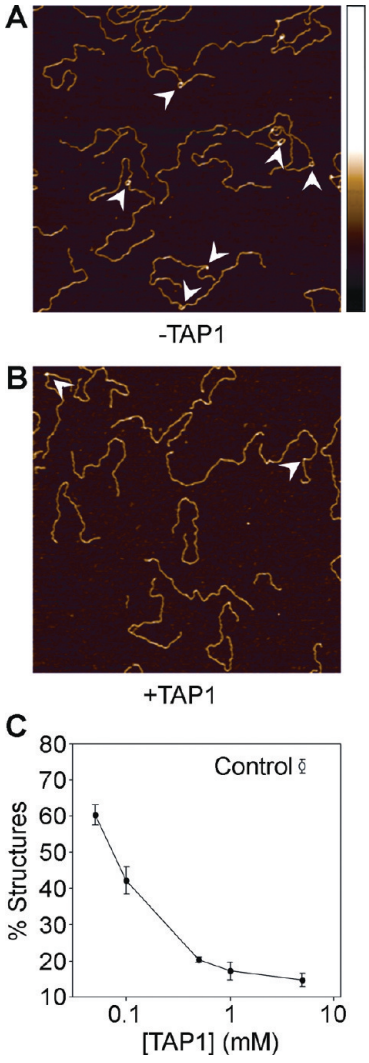

Figure 5. Effect of TAP1 on quadruplex stability. (A and B) Low-magnification (2 μm × 2 μm) images of plasmids that had been transcribed in the absence (A) or presence (B) of TAP1 (0.5 mM). The positions of structures are indicated by arrowheads. The shade height scale is 0–1.4 nm. (C) Dependence of the prevalence of structures on TAP1 concentration. Control (empty symbol) denotes the percentage of plasmids showing structures in the absence of TAP1. The data are from three independent experiments.

of varying concentrations of pyridostatin, linearized the plasmids, and subjected them to AFM imaging. As shown in Figure 4, transcribed plasmids had many structures, as usual (arrowheads, Figure 4A), but plasmids that had also been treated with RNase H showed very few structures (Figure 4B). In contrast, more structures were seen when the RNase H-treated plasmids had been incubated with pyridostatin [200 μM (arrowheads, Figure 4C)]. A frequency distribution of the volumes of structures seen after treatment with pyridostatin and RNase H is shown in Figure 4D. The peak volume was 194 ± 6 nm^3 (n = 100), similar to the values reported above for drug-free conditions. The concentration dependence of the effect of pyridostatin is shown in Figure 4E. Pyridostatin treatment increased the percentage of plasmids bearing structures from ~15 to ~30%, with half-maximal stimulation occurring at ~20 μM pyridostatin.

Effect of TAP1 on Quadruplex Stability. In contrast to pyridostatin, TAP1 has been reported to destabilize G-quadruplexes by disrupting the structural integrity of certain G-tetrads and potentially shows the opposite functional effect compared with that of a quadruplex-stabilizing ligand.[21] To test the effect of TAP1 in our system, we transcribed pPH600 in the absence and presence of TAP1 (0.5 mM) and counted the numbers of plasmids bearing structures. As shown in Figure 5A, the majority of control plasmids showed structures (arrowheads). In contrast, TAP1-treated plasmids showed far fewer structures (arrowheads, Figure 5B). The concentration dependence of the effect of TAP1 is shown in Figure 5C. TAP1 treatment reduced the percentage of plasmids bearing structures from ~75 to ~15%, with half-maximal inhibition occurring at ~0.1 mM TAP1.

DISCUSSION

In this study, we have provided direct structural evidence of the formation of G-quadruplex structures during transcription of a G-rich region within a 3.5 kbp plasmid. In addition, we have demonstrated the ability of small-molecule ligands to perturb the stability of these G-quadruplexes.

The single-chain antibody HF1 was originally selected from a phage library by screening against the biotinylated c-kit-2 G-quadruplex sequence immobilized on streptavidin.[17] When the plasmid encoding the gene for HF1 was expressed in human cell line HGC-27, the antibody had a widespread effect on gene expression within the cells. Specifically, of 18105 known protein-coding genes, 1767 were differentially expressed in cells containing HF1; of these, 55% were upregulated, whereas 45% were downregulated. Significantly, there was enrichment in putative G-quadruplex motifs at the beginning and end of the differentially expressed genes, suggesting that recognition of G-quadruplexes by HF1 can affect gene expression within the cells. Notably, however, this previous study did not demonstrate the specific physical interaction of HF1 with G-quadruplexes in the context of genomic DNA. In this study, we have transcribed a G-rich region of a plasmid and demonstrated the specific decoration of the structures formed in this region by HF1. Prior evidence had strongly suggested that the DNA structures produced were G-quadruplexes. HF1 binding was observed through the increase in the average volume of the structures, an increase that allowed us to estimate that on average several (approximately seven to eight) HF1 molecules bound to each structure.

PARP-1 is abundant in the chromatin of eukaryotic cells and is believed to function as a sensor of DNA strand breaks. Upon binding to DNA, PARP-1 polymerizes ADP-ribose onto nuclear acceptor proteins and in the process poly(ADP-ribosyl)ates itself. PARP-1 is also believed to recognize non-B-DNA structures in gene-regulating sequences and thereby control transcription. PARP-1 has previously been shown to bind to the c-kit-1 G-quadruplex.[18] This previous AFM analysis revealed an increase in the size of a 200 bp oligonucleotide bearing the c-kit-1 sequence, consistent with the addition of two molecules of PARP-1 to each G-quadruplex. In our experiments, the increase in molecular volume observed also suggested the binding of two to three molecules of PARP-1 to each G-quadruplex, in agreement with the previous result.[18] It is noteworthy that in this previous study the 200 bp oligonucleotide appeared as a blob in the AFM images, perhaps because of folding of the G-quadruplex; the DNA contour was not visible. The same study showed that the c-kit-1 oligonucleotide stimulated the poly(ADP-ribosyl)ation activity of PARP-1, a result that we have now replicated using a G-quadruplex generated during

dx.doi.org/10.1021/bi201600g | Biochemistry 2012, 51, 578–585

transcription. A striking finding of our AFM imaging experiments with PARP-1 was the reduction in the prevalence of looplike structures, with a corresponding increase in the frequency of spurs. These results suggest the binding of PARP-1 holds the two arms of the loop together to form a spurlike structure. Consistent with this idea, PARP-1 is known to be able to bind two DNA molecules simultaneously.[44]

The ability of pyridostatin to perturb the stability of G-quadruplexes was initially evaluated by FRET melting experiments using telomeric G-quadruplexes.[19] It was then shown to inhibit the binding of the protein POT1 (protection of telomeres 1) to a telomeric DNA sequence both in vitro and in living cells. Subsequent experiments showed that pyridostatin could reduce the translation efficiency of a reporter mRNA construct containing a G-quadruplex.[20] These observations suggest a specific stabilizing effect caused by binding of pyridostatin to G-quadruplexes. In our study, we have explicitly confirmed this stabilizing effect of pyridostatin on G-quadruplexes generated in the nontemplate strand during transcription of a G-rich sequence within plasmid pPH600. In contrast to the effect of pyridostatin, TAP1 was previously shown using CD and NMR spectroscopy to destabilize the structure of the two short G-quadruplex-forming sequences found in the promoter of c-kit and to increase the level of expression of c-kit in cell line HGC-27.[21] In our study, this destabilizing effect was demonstrated directly on the G-quadruplex generated during transcription of pH600.

Given the evidence that G-quadruplexes are involved in the control of gene expression, the availability of small molecules that are able to perturb their stability has major implications for the future production of novel anticancer agents. As mentioned above, the effects of some of these small molecules on gene transcription are now emerging. We suggest that the ability afforded by AFM to reveal the effects of these agents directly on known G-quadruplex structures formed in a biochemically functional context, as demonstrated here, will greatly assist in the future development of this therapeutic strategy.

■ ASSOCIATED CONTENT

Supporting Information

CD and thermal difference spectrum (TDS) analyses indicating the formation of G-quadruplexes in pPH600, frequency distributions of the molecular volumes of HF1 and PARP-1, and predicted locations of G-quadruplexes in pPH600. This material is available free of charge via the Internet at http://pubs.acs.org.

■ AUTHOR INFORMATION

Corresponding Author

*Phone: +44 1223 334014. Fax: +44 1223 334100. E-mail: jme1000@cam.ac.uk.

Funding

I.M. is supported by a Biotechnology and Biological Sciences Research Council Doctoral Training Award. R.K. is supported by a Deutscher Akademischer Austausch Dienst (DAAD) Postdoctoral Fellowship. The Balasubramanian lab is supported by program funding from Cancer Research UK and by project funding from the Biotechnology and Biological Sciences Research Council. R.M.H. and J.M.E. are grateful to Mr. and Mrs. C. Dobson for supporting their AFM imaging experiments.

■ ACKNOWLEDGMENTS

We are grateful to R. Rodriguez and Z. Waller for providing samples of pyridostatin and TAP1, respectively.

■ ABBREVIATIONS

AFM, atomic force microscopy; CD, circular dichroism; NMR, nuclear magnetic resonance; PARP-1, poly(ADP-ribose) polymerase-1; pPH600, plasmid derived from pBluescript KS(+) containing a fragment of the murine Sγ3 switch region; SDS−PAGE, sodium dodecyl sulfate−polyacrylamide gel electrophoresis; TDS, thermal difference spectrum.

■ REFERENCES

(1) Sannohe, Y., and Sugiyama, H. (2010) Overview of formation of G-quadruplex structures. *Current Protocols in Nucleic Acid Chemistry*, Chapter 17, Unit 17.2.1−17.2.17, Wiley, New York.

(2) Balasubramanian, S., Hurley, L. H., and Neidle, S. (2011) Targeting G-quadruplexes in gene promoters: A novel anticancer strategy? *Nat. Rev. Drug Discovery 10*, 261−275.

(3) Huppert, J. L., and Balasubramanian, S. (2005) Prevalence of quadruplexes in the human genome. *Nucleic Acids Res. 33*, 2908−2916.

(4) Oganesian, L., and Bryan, T. M. (2007) Physiological relevance of telomeric G-quadruplex formation: A potential drug target. *BioEssays 29*, 155−165.

(5) Smith, J. S., Chen, Q., Yatsunyk, L. A., Nicoludis, J. M., Garcia, M. S., Kranaster, R., Balasubramanian, S., Monchaud, D., Teulade-Fichou, M. P., Abramowitz, L., Schultz, D. C., and Johnson, F. B. (2011) Rudimentary G-quadruplex-based telomere capping in *Saccharomyces cerevisiae*. *Nat. Struct. Mol. Biol. 18*, 478−485.

(6) Siddiqui-Jain, A., Grand, C. L., Bearss, D. J., and Hurley, L. H. (2002) Direct evidence for a G-quadruplex in a promoter region and its targeting with a small molecule to repress c-MYC transcription. *Proc. Natl. Acad. Sci. U.S.A. 99*, 11593−11598.

(7) Huppert, J. L., and Balasubramanian, S. (2007) G-quadruplexes in promoters throughout the human genome. *Nucleic Acids Res. 35*, 406−413.

(8) Eddy, J., Vallur, A. C., Varma, S., Liu, H., Reinhold, W. C., Pommier, Y., and Maizels, N. (2011) G4 motifs correlate with promoter-proximal transcriptional pausing in human genes. *Nucleic Acids Res. 39*, 4975−4983.

(9) Law, M. J., Lower, K. M., Voon, H. P., Hughes, J. R., Garrick, D., Viprakasit, V., Mitson, M., De Gobbi, M., Marra, M., Morris, A., Abbott, A., Wilder, S. P., Taylor, S., Santos, G. M., Cross, J., Ayyub, H., Jones, S., Ragoussis, J., Rhodes, D., Dunham, I., Higgs, D. R., and Gibbons, R. J. (2010) ATR-X syndrome protein targets tandem repeats and influences allele-specific expression in a size-dependent manner. *Cell 143*, 367−378.

(10) Sarkies, P., Reams, C., Simpson, L. J., and Sale, J. E. (2010) Epigenetic instability due to defective replication of structured DNA. *Mol. Cell 40*, 703−713.

(11) De, S., and Michor, F. (2011) DNA secondary structures and epigenetic determinants of cancer genome evolution. *Nat. Struct. Mol. Biol. 18*, 950−955.

(12) Balasubramanian, S., and Neidle, S. (2009) G-quadruplex nucleic acids as therapeutic targets. *Curr. Opin. Chem. Biol. 13*, 345−353.

(13) Uribe, D. J., Guo, K., Shin, Y. J., and Sun, D. (2011) Heterogeneous nuclear ribonucleoprotein K and nucleolin as transcriptional activators of the vascular endothelial growth factor promoter through interaction with secondary DNA structures. *Biochemistry 50*, 3796−3806.

(14) Paeschke, K., Capra, J. A., and Zakian, V. A. (2011) DNA replication through G-quadruplex motifs is promoted by the *Saccharomyces cerevisiae* Pif1 DNA helicase. *Cell 145*, 678−691.

(15) Schaffitzel, C., Postberg, J., Paeschke, K., and Lipps, H. J. (2010) Probing telomeric G-quadruplex DNA structures in cells with in vitro

generated single-chain antibody fragments. *Methods Mol. Biol. 608*, 159−181.
(16) Monchaud, D., and Teulade-Fichou, M. P. (2008) A hitchhiker's guide to G-quadruplex ligands. *Org. Biomol. Chem. 6*, 627−636.
(17) Fernando, H., Sewitz, S., Darot, J., Tavaré, S., Huppert, J. L., and Balasubramanian, S. (2009) Genome-wide analysis of a G-quadruplex-specific single-chain antibody that regulates gene expression. *Nucleic Acids Res. 37*, 6716−6722.
(18) Soldatenkov, V. A., Vetcher, A. A., Duka, T., and Ladame, S. (2008) First evidence of a functional interaction between DNA quadruplexes and poly(ADP-ribose) polymerase-1. *ACS Chem. Biol. 3*, 214−219.
(19) Rodriguez, R., Müller, S., Yeoman, J. A., Trentesaux, C., Riou, J.-F., and Balasubramanian, S. (2008) A novel small molecule that alters shelterin integrity and triggers a DNA-damage response at telomeres. *J. Am. Chem. Soc. 130*, 15758−15759.
(20) Bugaut, A., Rodriguez, R., Kumari, S., Hsu, S.-T. D., and Balasubramanian, S. (2010) Small molecule-mediated inhibition of translation by targeting a native RNA G-quadruplex. *Org. Biomol. Chem. 8*, 2771−2776.
(21) Waller, Z. A. E., Sewitz, S. A., Hsu, S.-T. D., and Balasubramanian, S. (2009) A small molecule that disrupts G-quadruplex DNA structure and enhances gene expression. *J. Am. Chem. Soc. 131*, 12628−12633.
(22) Müller, S., Kumari, S., Rodriquez, R., and Balasubramanian, S. (2010) Small-molecule-mediated G-quadruplex isolation from human cells. *Nat. Chem. 2*, 1095−1098.
(23) Fernando, H., Rodriguez, R., and Balasubramanian, S. (2008) Selective recognition of a DNA G-quadruplex by an engineered antibody. *Biochemistry 47*, 9365−9371.
(24) Rangan, A., Fedoroff, O. Y., and Hurley, L. H. (2001) Induction of duplex to G-quadruplex transition in the c-myc promoter region by a small molecule. *J. Biol. Chem. 276*, 4640−4646.
(25) Hounsou, C., Guittat, L., Monchaud, D., Jourdan, M., Saettel, N., Mergny, J. L., and Teulade-Fichou, M. P. (2007) G-quadruplex recognition by quinacridines: A SAR, NMR, and biological study. *ChemMedChem 2*, 655−666.
(26) Campbell, N. H., Patel, M., Tofa, A. B., Ghosh, R., Parkinson, G. N., and Neidle, S. (2009) Selectivity in ligand recognition of G-quadruplex loops. *Biochemistry 48*, 1675−1680.
(27) Tran, P. L., Largy, E., Hamon, F., Teulade-Fichou, M. P., and Mergny, J. L. (2011) Fluorescence intercalator displacement assay for screening G4 ligands towards a variety of G-quadruplex structures. *Biochimie 93*, 1288−1296.
(28) Crampton, N., Roes, S., Dryden, D. T. F., Rao, D. N., Edwardson, J. M., and Henderson, R. M. (2007) DNA looping and translocation provide an optimal cleavage mechanism for the type III restriction enzymes. *EMBO J. 26*, 3815−3825.
(29) Crampton, N., Yokokawa, M., Dryden, D. T. F., Edwardson, J. M., Rao, D. N., Takeyasu, K., Yoshimura, S. H., and Henderson, R. M. (2007) Fast-scan atomic force microscopy reveals that the type III restriction enzyme EcoP15I is capable of DNA translocation and looping. *Proc. Natl. Acad. Sci. U.S.A. 104*, 12755−12760.
(30) Neaves, K. J., Cooper, L. P., White, J. H., Carnally, S. M., Dryden, D. T. F., Edwardson, J. M., and Henderson, R. M. (2009) Atomic force microscopy of the EcoKI type I DNA restriction enzyme bound to DNA shows enzyme dimerisation and DNA looping. *Nucleic Acids Res. 37*, 2053−2063.
(31) Neaves, K. J., Huppert, J. L., Henderson, R. M., and Edwardson, J. M. (2009) Direct visualization of G-quadruplexes in DNA using atomic force microscopy. *Nucleic Acids Res. 37*, 6269−6275.
(32) Duquette, M. L., Handa, P., Vincent, J. A., Taylor, A. F., and Maizels, N. (2007) Intracellular transcription of G-rich DNAs induces formation of G-loops, novel structures containing G4 DNA. *Genes Dev. 18*, 1618−1629.
(33) Bardin, C., and Leroy, J. L. (2008) The formation pathway of tetramolecular G-quadruplexes. *Nucleic Acids Res. 36*, 477−488.
(34) Scott, D. W. (1979) On optimal and data-based histograms. *Biometrika 66*, 605−610.
(35) Welch, B. L. (1947) The generalization of 'Student's' problem when several different population variances are involved. *Biometrika 34*, 28−35.
(36) Schneider, S. W., Lärmer, J., Henderson, R. M., and Oberleithner, H. (1998) Molecular weights of individual proteins correlate with molecular volumes measured by atomic force microscopy. *Pfluegers Arch. 435*, 362−367.
(37) Cantor, C. R., and Schimmel, P. R. (1980) *Biophysical Chemistry. Part II. Techniques for the Study of Biological Structure and Function*, W. H. Freeman and Co., New York.
(38) Edstrom, R. D., Meinke, M. H., Yang, X., Yang, R., Elings, V., and Evans, D. F. (1990) Direct visualization of phosphorylase-phosphorylase kinase complexes by scanning tunneling and atomic force microsopy. *Biophys. J. 58*, 1437−1448.
(39) Oncley, J. L., Scatchard, G., and Brown, A. (1947) Physical-chemical characteristics of certain of the proteins of normal human plasma. *J. Phys. Colloid Chem. 51*, 184−198.
(40) Durschchlag, H., and Zipper, P. (1997) Calculation of partial specific volumes and other volumetric properties of small molecules and polymers. *J. Appl. Crystallogr. 30*, 803−807.
(41) Grant, E. H. (1957) The dielectric method of estimating protein hydration. *Phys. Med. Biol. 2*, 17−28.
(42) Hori, K., Takahashi, T., and Okada, T. (1998) The measurement of exonuclease activities by atomic force microscopy. *Eur. Biophys. J. 27*, 63−68.
(43) Kikin, O., D'Antonio, L., and Bagga, P. S. (2006) QGRS Mapper: A web-based server for predicting G-quadruplexes in nucleotide sequences. *Nucleic Acids Res. 34*, W676−W682.
(44) Rolli, V., Ruf, A., Augustin, A., Schulz, G. E., Ménissier-de Murcia, J., and de Murcia, G. (2000) Poly(ADP-ribose) polymerase: Structure and function. In *From DNA Damage and Stress Signalling to Cell Death: Poly ADP-Ribosylation Reactions* (de Murcia, G., and Shall, S., Eds.) pp 35−79. Oxford University Press, New York.